Large scale fabrication of nitrogen vacancy embedded diamond nanostructures for single photon source application

Qianqing Jiang (姜倩晴)[1], Wuxia Li (李无瑕)[1], Chengchun Tang (唐成春)[1], Yanchun Chang (常彦青)[1], Tingting Hao (郝婷婷)[1], Xinyu Pan(潘新宇)[1], Haitao Ye(叶海涛)[3], Junjie Li (李俊杰)[1], and Changzhi Gu (顾长志)[1,2]

[1]Beijing National Laboratory of Condensed Matter Physics, Institute of Physics, Chinese Academy of Sciences, Beijing, 100190, China
[2]Collaborative Innovation Center of Quantum Matter, Beijing, 100190, China
[3]School of Engineering and Applied Science, Aston University, Birmingham B4 7ET, United Kingdom

Keywords: Large scale, nitrogen vacancy, diamond, single photon source

Corresponding authors. E-mail: liwuxia@iphy.ac.cn; czgu@iphy.ac.cn

PACS: 81.16.-c, 87.85.Rs, 81.07.-b

Abstract

Color centers in diamond are prominent candidates to generate and manipulate quantum states of light, even at room temperature. However, the efficiency of photon collection efficiency in bulk diamond is greatly reduced by the refraction at diamond/air interface. To address this issue, arrays of diamond nanostructures of different diameters and top end shapes have been fabricated with HSQ, PMMA and Cr as the etching masks, towards large scale fabrication of nitrogen vacancy (NV) embedded diamond single photon sources with enhanced collection efficiency. With mixture of O_2 and CHF_3 gas plasma, diamond pillars with diameter down to 45 nm have been achieved. The top end shape evolution has also been traced with a simple model. The tests of size dependent single photon properties confirmed a best single photon collection efficiency enhancement with a factor larger than ten folds and a mild decreasing of the decoherence time with the reduction of the pillar diameter was observed as expected. These results provide useful information in future applications of nanostructured diamond as single photon sources.

1. Introduction:

Diamond is an important material for its outstanding properties [1-3] and has drown more and more interest from researchers world-widely for its novel physical and optical properties and promising applications in areas such as single photon source, high-sensitivity sensors and information processing, benefit from the naturally existed or artificially introduced abundant color centers [4-14]. Of particular interest is the electron spin of NV− centers in diamond, which can be initialized, coherently controlled, and read out at room temperature [7]. The robust spin coherence [9] and optical addressability via spin-dependent orbital transitions [10] offer such systems with great potential in applications ranging from quantum information processing [11-14] to nanoscale electric field sensing [5-17].

However, in bulk diamond crystals, it has the disadvantage of low photon out-coupling, that is the total reflection effect at the diamond-air interface results in tremendous loss of the fluorescence photon counting rate. To address this problem, theoretical and experimental work has been performed to investigate the size and geometry effect on the single photon collection efficiency of NV embedded diamond structures. In particular, different micro/nano structures like hemisphere and nanowires have been fabricated out of diamond substrates to improve the in- and out-coupling of photons, to facilitate the manipulation of the light–matter interactions [18-20], and for more efficient excitation, higher collection efficiency and single photon flux [21]. For size effect study, thin and high aspect ratio nanowires covered with a graphic or carbonaceous shell has been obtained through a chemical vapor deposition (CVD) process [22]. Diamond fibers with various diameters were fabricated by top-down method and the best shape of diamond nanowires was predicted by simulations. The optical coupling

of the NV center emission (at λ=637nm) to diamond nanowire has been modeled using FDTD simulations [23]. The best coupling efficiency turned out to be the largest for nanowires with diameters between 180 nm and 220 nm [24, 25]. In addition, in a recent work, the effect of the morphology of nanowire on the single photon collection efficiency enhancement is reported on nanowire of conic shape, a net photon flux exceeds 1.5×10^6 /s was achieved [25]. Nevertheless, optimized fabrication approach for large scale diamond micro-/nanostructures with tunable geometry, size and distribution is still highly demanded [26].

In this paper, we adopted a combined technique of electron beam lithography (EBL) followed by induction couple plasma (ICP) - reactive ion etching (RIE) to fabricate diamond nanopillars with various sizes and top shapes. Thin diamond nanopillars with diameter down to 45 nm and aspect ratio up to 20 were prepared. The nanopillar top end geometry evolution process during etching was studied systematically. The dependency between the fluorescence photon collection rate of NV center and the nanopillar diameter was also probed. Single photons count rate measurement indicates an enhancement of about ten folds in the photon collection efficiency compared with the un-sculptured diamond crystal. The $g^{(2)}(\tau)$ and Ramsey fringes measurements showed that the RIE processing didn't affect the single photon emission and the coherent properties. Size effect was examined and the underlying mechanism is discussed.

2. Methods

Two kinds of fabrication processes, using HSQ negative resist (Figure 1(a) or PMMA

positive photoresist (Figure 1(b)), were adopted in the experiment. As for the prior approach, firstly, HSQ was spin-coated on cleaned diamond surface. Then electron beam lithography (EBL) was performed. For EBL processing, the accelerating voltage was set to 100 keV and the dose varied with the pattern size. For circles larger than 80 nm in diameter, the applied dose was 1600 μC/cm^2. For smaller circles, the applied dose was 2500 μC/cm^2. After developing, the silicon oxide patterns were used as masks for the following reactive ion etching (RIE) treatment, in which gas mixture of CHF3: O2 (4.2: 30 sccm) was used. During RIE procedure, the chamber pressure was 10 mTorr and the RF power was 100 W. After RIE etching, the remaining masks were wiped off in diluted HF solution and the diamond nanopillars were finally achieved.

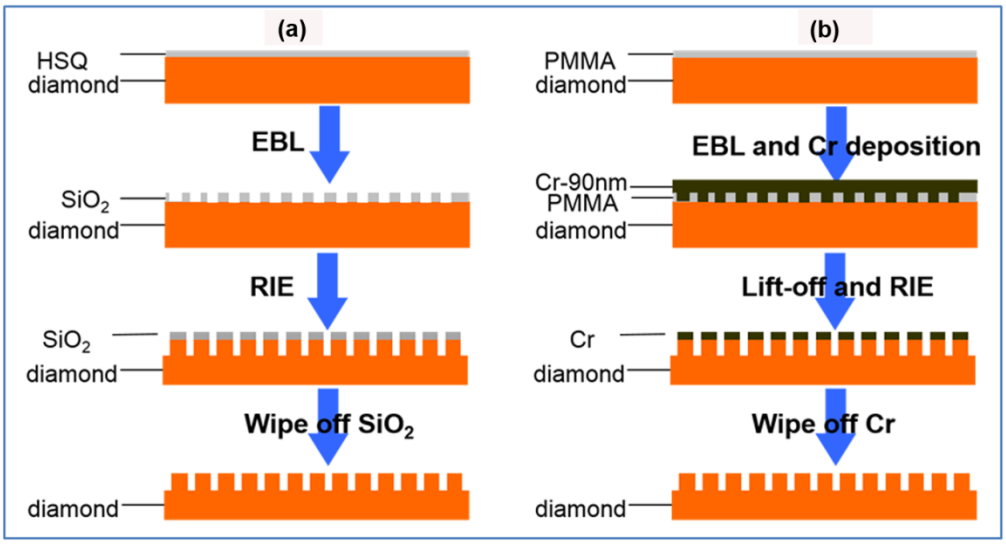

Fig. 1. Top-down fabrication of diamond nanostructure arrays by electron beam lithography related techniques: (a) HSQ negative resist approach; (b) PMMA positive resist approach.

As for the PMMA approach, again, a layer of 300 nm PMMA was spin-coated on cleaned diamond surface. Then circle patterns were exposed with EBL and developed. Thereafter, a 90 nm thick Cr was deposited with thermal evaporation system, which was followed by

lift-off in acetone to obtain Cr circular masks. Different from the first approach, rather than using the developed resist as the masks, here a pattern transfer process, metal deposition and lift-off was used. After RIE processing, the Cr was further removed to get diamond nanopillars.

The fluorescence scanning and the single photon count rate measurement was carried on a home-built laser scanning confocal microscope system which can detect single photon fluorescence and has sub-micrometer precision. During measurement, a 532-nm continuous wave laser beam was switched on and off by an acoustic optical modulator (AOM); an X-Y galvanometer was used to control the scanning of the laser spot before it was directed to the sample through a microscope objective. The spin state-dependent fluorescence of the NV− centre was collected by the same objective, which was then filtered by a 532 nm notch and a 650 nm long path. After that, the weak light signal was translated into the electronic pulse signal by a single-photon counting module and was subsequently counted by a pulse counter or to a Hanbury-Brown and Twiss detection system to record the second order intensity correlation function [$(g^{(2)}(\tau)$].

3. Results and discussion

3.1 Fabrication of diamond nanostructure arrays

Diamond nanopillar arrays of various diameters and periods have been prepared with the HSQ approach. First of all, the effect of the period of the patterns was examined. In that for a particular value of diameter, patterns with period set twice, threefold, fivefold and tenfold were prepared. For the developed cylindrical masks of small diameter, we found that only

arrays of small periods can stand straight. Specifically, pillars with diameter of 50 nm and 80 nm are easy to “fall down” on the substrate when the period is larger than threefold of the diameters. Fig.2(a) shows the pillar mask array of 50 nm diameter with a period of 100 nm, which stands well. For pillars wider than 100 nm, the period can be set larger, as shown in Fig.2(b), the pillars are 300 nm in diameter and the period is 1.5 μm.

With PMMA approach, Cr mask arrays of different diameter and period were also prepared. Pillar mask arrays with diameter of 80 nm, period of 160 nm, and diameter of 250 nm, period of 500 nm are shown in Fig.3. Compared with PMMA approach, pillar masks prepared with HSQ have better cylindrical shape and the diameter can be smaller, since the Cr mask size is limited by the lift-off process, which has a minimum value of 80 nm.

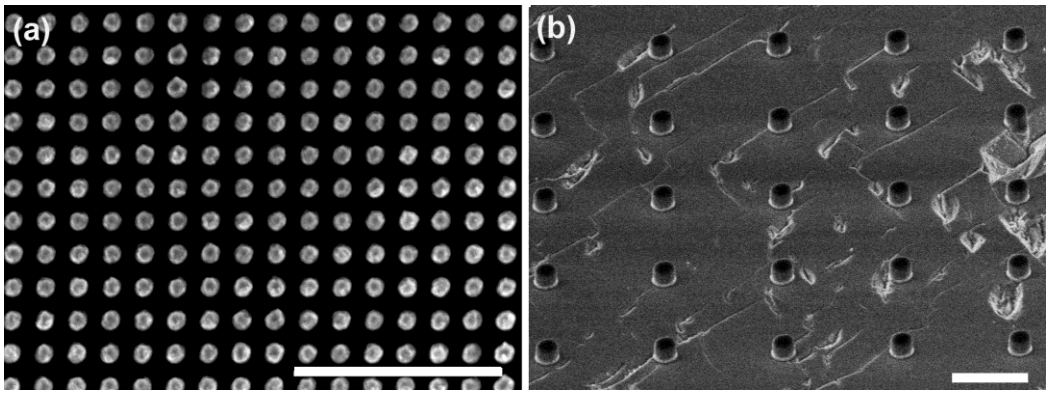

Fig. 2. Masks of different periods prepared with the HSQ negative resist approach: (a) Diameter 50 nm, period 100 nm; (b) Diameter 300 nm, period 1.5 μm.The scale bar is 2 μm.

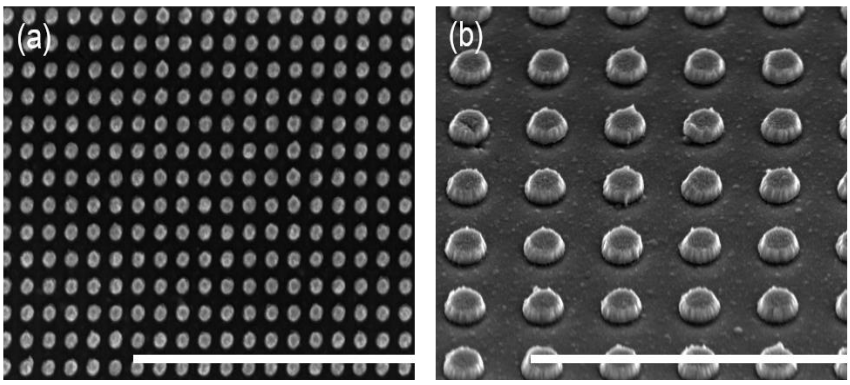

Fig. 3. Masks of different periods prepared with the PMMA positive resist approach: (a)

Diameter 80 nm, period 160 nm; (b) Diameter 250 nm, period 500 nm. The scale bar is 2 μm.

Diamond nanopillar arrays of different diameter and period were then prepared in RIE system with both HSQ (Fig.4) and PMMA approach (Fig.5). It should be mentioned that ultra-thin diamond nanopillars with diameter of 45 nm, period of 100 nm and height of about 900 nm were prepared with HSQ approach (Fig.4(a)). The length-diameter ratio reached as high as 20. For pillars of such small diameter, the maximum array period should not exceed twice of the diameter of the masks, otherwise, the resulted pillar masks are easy to "fall down". Pillar arrays of 100 nm and 500 nm in diameter prepared with HSQ was shown in Fig.4(b) and (c). It's clear that they all have a conical top-end.

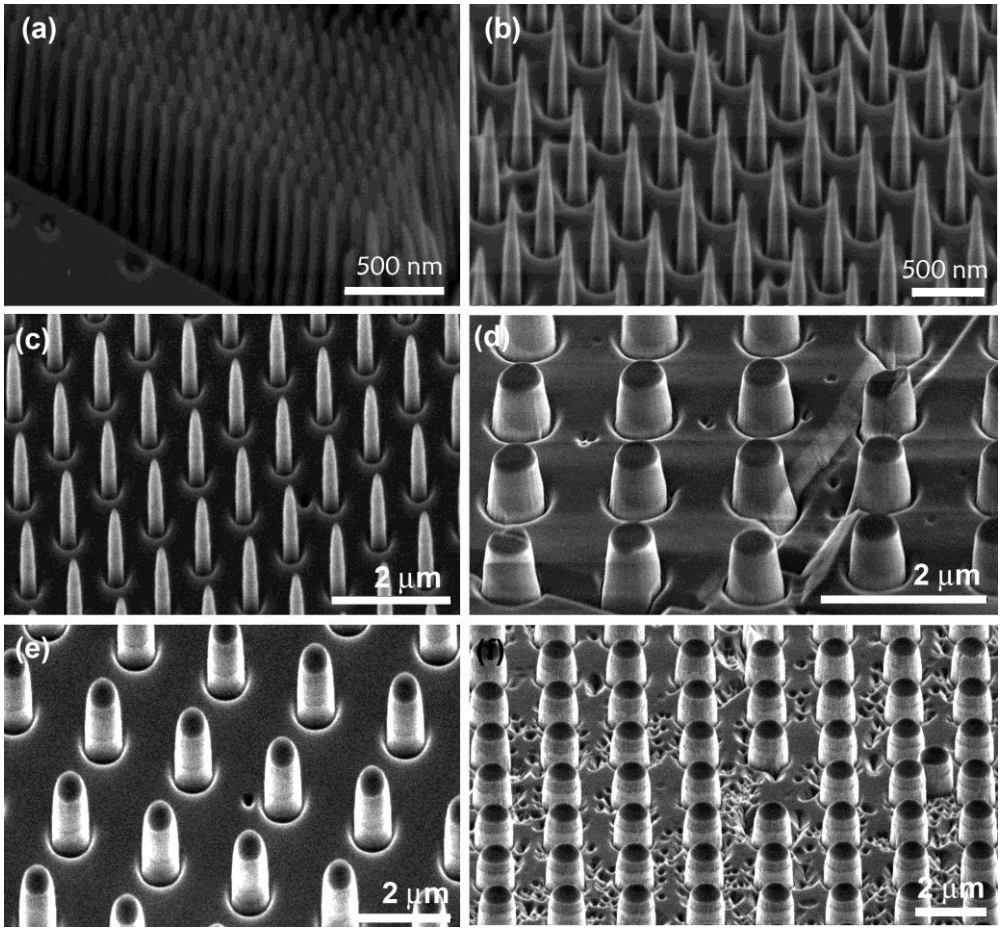

Fig. 4. Pillars fabricated with the HSQ negative resist approach that having diameters and . periods of: (a) 50 nm, 100 nm; (b) 100 nm, 500 nm; (c) 220 nm, 500nm; (d) 730 nm, (e) 500

nm, 1.5μm; (f) . 1.0 μm, 1.0 μm.

Diamond nanopillars prepared with PMMA approach are also shaped with conical top-end (Fig.5). From Fig. 5 (a) and (b), in which the periods are both 1.5 μm, while the diameter is of 300 nm and 250 nm, it can be seen that the cone angle was smaller with thinner pillars.

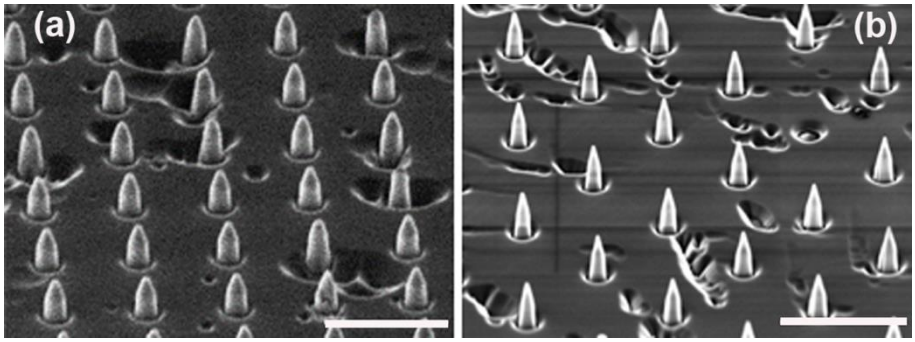

Fig. 5. Cone structure on top end of the pillars: (a) Diamond pillar array of diameter 300 nm, period 1.5 μm fabricated with the HSQ approach; (b) Diamond pillar array with pillar diameter of 250 nm, period 1.5 μm fabricated through the PMMA approach. The scale bar is 2 μm.

To find out the relationship between the cone angle and the mask material, more detailed experiment was taken. The cone angle of pillars prepared with both Cr and HSQ masks were measured as shown in Fig.6. All the pillars are 100 nm in diameter in image (a). It's clear that the cone angle of pillars with a certain diameter increases with the period and saturated at a certain value. We attribute this phenomenon to the etching rate, which is closely related to the mask pattern intensity. When the masks stand closely, the incident ions scattered by the etched structures and strike the nearby pillars, which may hinder the cone angle formation.

It should also be noticed that, cone angle of pillars prepared by HSQ approach has a smaller change range and the saturation value is just half of those prepared with Cr mask.

Such difference mainly comes from the initial tomography of the two masks. By comparison of HSQ mask and Cr mask shown in Fig.2(b) and Fig.3(b) respectively, we can see that the HSQ mask has a steep sidewall while the Cr mask has a pre-existing cone angle. In the following etching process, the cone angle was gradually enlarged and the initial difference was kept or even magnified. Larger cone angle was finally obtained for pillars fabricated with Cr mask. The cone angle variation with pillar diameter was further studied with pillars fabricated using HSQ as the etching mask, and the pattern period was three times of the values of the diameter. As shown in Fig.6 (b), the cone angle increases with the pillar diameter until it saturates at an angle of about 18 degrees.

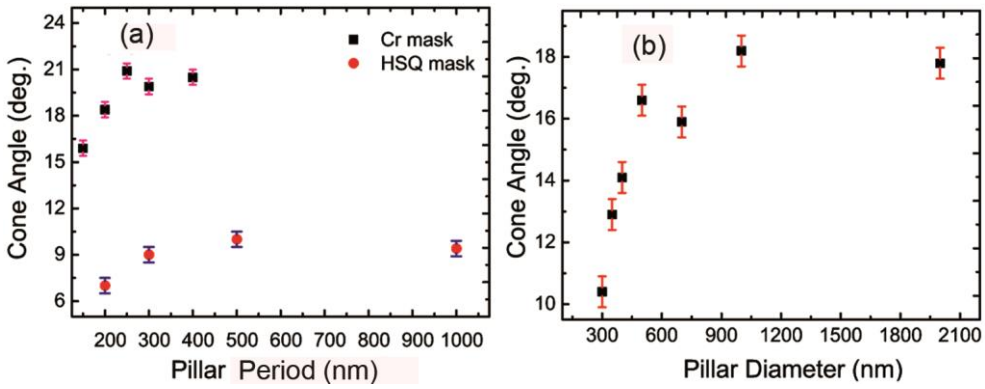

Fig. 6. Cone angle variation trends: (a) the effect of mask type and the mask pattern period. The measured pillars are 100 nm in diameter; (b) the effect of the mask diameter, here the pillar period is three times in value of that of the pillar diameter.

For better understanding, the cone angle evolution during the etching process was investigated and a simple model was then proposed. At first, diamond pillar array of different diameters was first etched using the PMMA approach in which Cr mask was used (Fig.7(a)). With all residual mask material removed, long time etching was then taken, during which the top-end cone angle of the aimed pillars was checked at 70, 130, 160, and 310 min of the process. For pillars of 200 nm in diameter, the SEM images of different etching time are

shown in Fig.7 (b) - (c). As we can be seen from these images, the top-end cone angle was unchanged when it has been formed on the pillar, while the pillar height was gradually decreased as the etching going on. For pillar of 1 μm in diameter, the cone angle was enlarged when the etching time was changed from 70 min to 310 min, as shown in the SEM image in Fig.7 (f) and (g). As mentioned before, the residual mask material had been removed after 70 minutes etching. Which means the following etching was taken on pre-formed pillars without any mask.

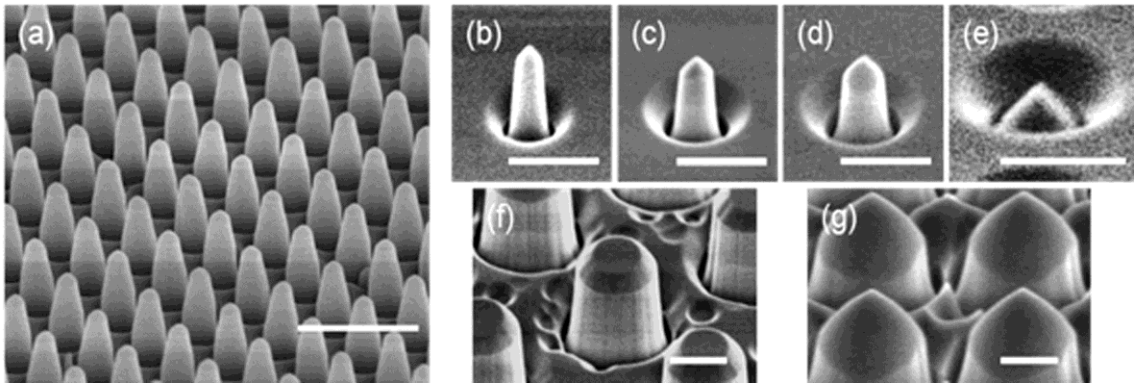

Fig. 7. The effect of the etching time on the top shape of pillars: (a) Diamond pillar array fabricated with the PMMA approach; (b) - (e) Tomography evolution of a 200 nm diameter pillar when the etching time was set at 70 min, 130 min, 160 min and 310 min; (f), (g) Tomography evolution of a 1μm diameter pillar when the etching time was sent 70 min and 310 min, respectively.

Based on the experiment results discussed above, a conical top end evolution mode of diamond pillars prepared by RIE is proposed here. In details, the process is roughly divided into three stages (Fig.8). At the initial stage, with the bombing of the incident reactive ions, small facet forms at the edge of the cylindrical mask, shown as inclined line A B in Fig.8 (a), and a circular truncated cone appears. With the etching going on, the facet expands and the cone angle increases till the pillar mask is cone shaped (Fig.8 (b)). Then the tapered facets going down into the diamond pillar at a certain etching rate, till the end of the etching process

or the mask material is totally consumed (Fig.8 (c)).

For pillar of smaller diameter, conical shape mask would be formed earlier than the thicker ones. Cone angle of the latter is still increasing while the former one becomes fixed. In this way, larger cone angle can be obtained for thicker pillars, as we discussed in Fig.6 (b). When we removed the mask on the top end at 70 min etching, conical shape had already formed on small pillars (Fig.7 (b)) while larger ones still had a circular truncated conical top end (Fig.7 (f)). The cone angle would keep fixed for the former, while it would continue to expand for the latter.

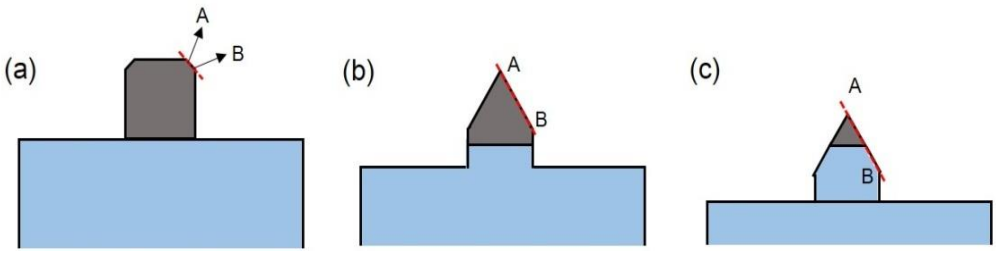

Fig. 8. The top shape evolution process of the etch pillars: (a) Facet forming at the edge of a cylindrical mask; (b) Expending of the facet on the etched pillar; (c) Formation of conical top end.

3.2 Single photon properties of nanostructured diamonds

For single photon properties measurement, pillars with diameter from 150 nm to 1 μm were finally prepared on a piece of 1 ppm diamond with proper distribution of single NV centers by the HSQ approach. In the confocal scanning imaging process, obvious brighter spots can be picked, positioned and confirmed as NV center emission. The second order autocorrelation function measurement further verified the single photon emission property. The relation between the single photon collection efficiency enhancement and the diameter of

the pillar was then studied. Pillar arrays of varied diameters were scanned and the single photon counting rate was compared. The single photon counting rate from NV center in pillars with a certain diameter fluctuates. To take pillars of 800 nm in diameter as an example, the largest counting rate was 380 kcounts/s, while the smallest was 270 kcounts/s. The inset of Fig.9 gives the largest measured counting rate of NV center in pillars with each diameter value from 150 nm to 1 μm. The highest enhancement about 10 folds was got at 650 nm diameter which drifts from the simulation results in previous report [5] while the relation between the counting rate and the diameter is not that obvious. We attribute this result to the pillar shape which has a conical top end fabricated with the RIE system and the randomness of the NV center position in the pillars which may departs from the pillar center.

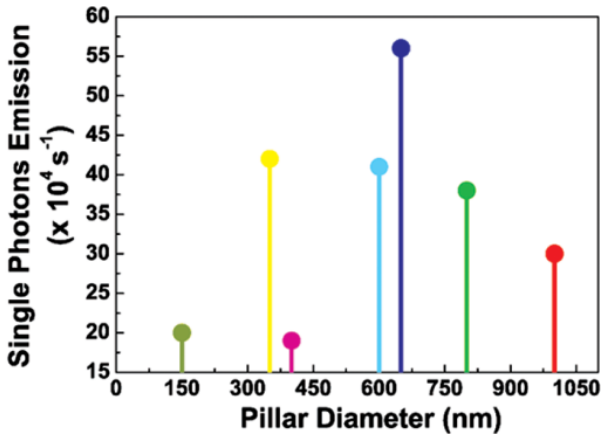

Fig. 9. The single NV center emission count rate for pillars of different diameters.

Decoherence time (T_2*) measurement was then taken on pillars of varied diameters. T_2* of NV center clusters in different pillars of the same diameter differs from each other as the circumstance in/out the pillars varies. For instance, T_2* of NV center clusters at room temperature in 860 nm pillars changes between 500 ns and 700 ns (Fig.10 (a)). In our experiment, several pillars of a same diameter were measured at room temperature and the

average value of T_2* was taken to make a contrast between pillars of different diameters. It comes out that, T_2* of NV center clusters in diamond nanopillars decreases with the pillar diameter (Fig.10 (b)). This dependency can be contributed to the circumstance near the diamond pillar surface. During the pillar etching, reactive ions bombed at the pillar surface which may introduce a large number of defects such as atom replacement and vacancies to a certain depth into the pillar. Together with dangling bonds on the pillar surface, these defects alter the local electromagnetic environment of the NV centers near the pillar surface and disturb the electron spin of the centers, which finally shorten the T_2* of the centers. As the pillar diameter decreases, a greater proportion of the NV centers distribute near the pillar surface and defects near the pillar surface can make greater impact. Therefore, we observed decreased T_2* for centers with reduced pillar diameters.

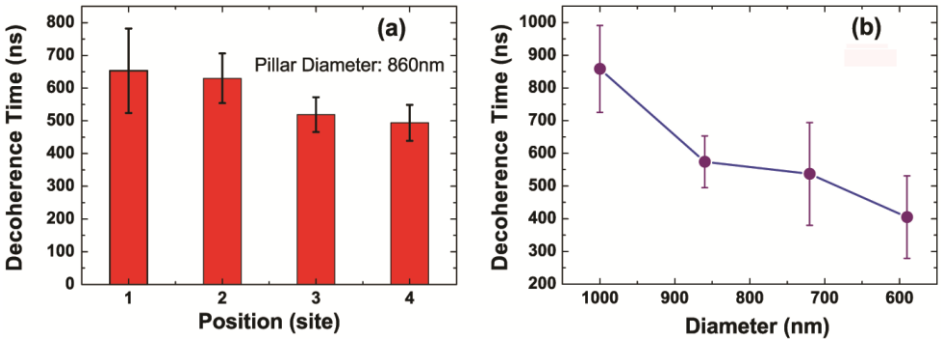

Fig. 10. (a) Decoherence time of NV center clusters in four diamond pillars of 860 nm in diameter.; (b) Pillar diameter dependent average Decoherence time.

4. Conclusions

To sum up, we show effective fabrication of diamond nanopillars of varied diameters with both HSQ and PMMA approaches using RIE. Ultra-thin pillars of 45 nm in diameter and high/diameter ratio of 20 were obtained with the HSQ approach. We find that conical top end

can be formed and the cone angle changes with the mask material, the period and diameter of the pillars. A facet etching mode is then proposed to explain the top shape evolution trends. The size dependent single photon collection efficiency of NV centers buried in the diamond pillars was investigated. It was found that the best enhancement factor was larger than 10 folds. The measurement also shows variation of the decoherence time of pillars with the same diameter, which might be correlated to the pillar shape and the randomness of the position of NV centers. However, a mild decreasing of the decoherence time with the reduction of the pillar diameter has been observed, which is as expected. Our results could provide very useful information in future applications of nanostructured diamond as single photon sources.

Acknowledgments

The authors thank Gangqing Liu for help with the single photon source measurement. This work is supported by the National Natural Science Foundation of China under Grants Nos. 11574369, 11574368, 91323304, 11174362, 51272278 and the FP7 Marie Curie Action (project No 295208) sponsored by European Commission.

References

[1] Brookes C. A. 1970 Nature **228** 660.

[2] Faklaris O, Joshi V, Irinopoulou T, Tauc P, Sennour M, Girard H, Gesset C, Arnault J-C, Thorel A, Boudou J-P, Curmi P A, and Treussart F 2009 AcsNano **3** 3955.

[3] Luo D, Wu L, Zhi J 2009 AcsNano **3** 2121.

[4] Maze J R, Stanwix P L, Hodges J S, Hong S, Taylor J M, Cappellaro P, Jiang L, Dutt M V, Togan E, Zibrov A S, Yacoby A, Walsworth R Land Lukin M D 2008 Nature **455** 644.

[5] Robledo L, Childress L, Bernien H, Hensen B, Alkemade P F.and Hanson R 2011 Nature **477** 574.

[6] Bernien H, Childress L, Robledo L, Markham M, Twitchen D and Hanson R 2012 Phys. Rev.Lett. **108**, 043604.

[7] Kurtsiefer C, Mayer S, Zarda P and Weinfurter H 2000 Phys. Rev.Lett. **85** 290.

[8] Jelezko F, Gaebel T, Popa I, Gruber A and Wrachtrup J 2004 Phys. Rev. Lett. **92** 076401.

[9] Balasubramanian G, Neumann P, Twitchen D, Markham M, Kolesov R, Mizuochi N, Isoya J, Achard J, Beck J, Tissler J, 2009 Nat. Mater. **8** 383.

[10] Gruber A, Dra ̈benstedt A, Tietz C, Fleury L, Wrachtrup J Borczyskowski C 1997 Science **276** 2012.

[11] Dutt M V, Childress L, Jiang L, Togan E, Maze J, Jelezko F, Zibrov A S, Hemmer P R, Lukin M D 2007 Science **316** 1312.

[12] Neumann P, Beck J, Steiner M, Rempp F, Fedder H, Hemmer P R, Wrachtrup J and Jelezko F 2010 Science **329** 542.

[13] Buckley B B, Fuchs G D, Bassett L C and Awschalom D D 2010 Science **330** 1212..

[14] Robledo L, Childress L, Bernien H, Hensen B, Alkemade P F A and Hanson R 2011 Nature **477** 574.

[15] Maze J R, Stanwix P L, Hodges J S, Hong S, Taylor J M, Cappellaro P, Jiang L, Dutt M V G, Togan E, Zibrov A S 2008 Nature **455** 644.

[16] Balasubramanian G, Chan IY, Kolesov R, Al-Hmoud M, Tsisler J, Shin C, Kim C, Wojcik A, Hemmer P R, Krueger A 2008 Nature **455** 648.

[17] Dolde F, Fedder H, Doherty M W, No ̈bauer T, Rempp F, Balasubramanian G, Wolf T, Reinhard F, Hollenberg L C L, Jelezko F 2011 Nat. Phys. **7** 459.

[18] Hausmann B J M, Khan M, Zhang Y, Babinec T M, Martinick K, McCutcheon M, Hemmer P R and Lončar M 2010 Diam.Relat.Mater. **19** 621.

[19] Baik E-S, baik Y-J, Lee S W, Jeon D 2000 Thin Solid Films **377** 295.

[20] Tao Y, Degen C 2013 Adv. Mater. **25** 3962.

[21] Babinec T M, Hausmann B J, Khan M, Zhang Y, Maze J R, Hemmer P R, Loncar M 2010 Nature Nanotech **5** 195.

[22] Hsu C-H and Xu J 2012 Nanoscale **4** 5293.

[23] Hausmann B J M, Khan M, Zhang Y 2010 Diamond and Related Materials **19** 621.

[24] Hausmann B J M, BabinecT M, Choy J T 2011 J. Phys. **13** 045044.

[25] Momenzadeh S A, Stöhr R J, de Oliveira F F 2014 Nano letters **15** 165.

[26] Castelletto S, Harrison J P, Marseglia L, Stanley-Clarke A C, Gibson B C, Fairchild B A, Hadden J P, Ho Y L D, Hiscocks M P, Ganesan K, Huntington S T, Ladouceur F, Greentree A D, Prawer S, O'Brien J L, Rarity J G 2011 New. J. Phys. **13** 025020.